Binding of Divalent Cations to Acetate:

Molecular Simulations Guided by Raman Spectroscopy

Denilson Mendes de Oliveira[1], Samual R. Zukowski[1], Vladimir Palivec[2], Jérôme Hénin[3,4], Hector Martinez Seara[2], Dor Ben-Amotz[1*], Pavel Jungwirth[2*], Elise Duboué-Dijon[2,3,4*]

[1] *Department of Chemistry, Purdue University, West Lafayette, Indiana 47907*

[2] *Institute of Organic Chemistry and Biochemistry, Academy of Sciences of the Czech Republic, Flemingovo nám. 2, 16610 Prague 6, Czech Republic*

[3] *CNRS, Université de Paris, UPR 9080, Laboratoire de Biochimie Théorique, 13 rue Pierre et Marie Curie, 75005, Paris, France*

[4] *Institut de Biologie Physico-Chimique-Fondation Edmond de Rothschild, PSL Research University, Paris, France*

*email: *pavel.jungwirth@uochb.cas.cz; bendor@purdue.edu; duboue-dijon@ibpc.fr*

Abstract

In spite of the biological importance of the binding of Zn^{2+}, Ca^{2+}, and Mg^{2+} to the carboxylate group, cation-acetate binding affinities and binding modes remain actively debated. Here, we report the first use of Raman multivariate curve resolution (Raman-MCR) vibrational spectroscopy to obtain self-consistent free and bound metal acetate spectra and one-to-one binding constants, without the need to invoke any *a priori* assumptions regarding the shapes of the corresponding vibrational bands. The experimental results, combined with classical molecular dynamics simulations with a force field effectively accounting for electronic polarization via charge scaling and *ab initio* simulations, indicate that the measured binding constants pertain to direct (as opposed to water separated) ion pairing. The resulting binding constants do not scale with cation size, as

1

the binding constant to Zn^{2+} is significantly larger than that to either Mg^{2+} or Ca^{2+}, although Zn^{2+} and Mg^{2+} have similar radii that are about 25% smaller than Ca^{2+}. Remaining uncertainties in the metal acetate binding free energies are linked to fundamental ambiguities associated with identifying the range of structures pertaining to non-covalently bound species.

1 Introduction

Divalent non-transition metal cations, in particular calcium (Ca^{2+}), magnesium (Mg^{2+}), and zinc (Zn^{2+}), play important roles in many biological processes and diseases.[1–10] Calcium is one of the key signaling species triggering changes in conformations of proteins involved, among others, in interactions between neurons, contraction of muscle cells, or exocytosis.[1,2] Magnesium is vital, for example, for enzymatic catalysis including ATP synthesis and for stabilizing nucleic acids.[3–5] Similarly, zinc is essential for proper function of many enzymes involved, e.g., in cell growth and reproduction, as well as for DNA stability and gene expression.[6,7] The biological functions of these ions are realized by specialized ion-binding structures of the relevant biomolecules, such as the calcium-binding EF-hand motif[8] and the zinc finger[9] in proteins or phosphate-containing nucleic acid backbone motifs for binding of magnesium.[10] Carboxylate of the side chain of glutamate or aspartate, or monovalent phosphate of the DNA/RNA backbone of phosphorylated biomolecules are examples of biologically relevant negatively charged groups that interact with divalent cations. Here, we focus on the former group with the aim to elucidate the structural and energetic details of the interaction between an acetate anion—previously shown to be a good proxy for ion pairing of biologically relevant carboxylate groups[11]—with $Ca^{2+}/Mg^{2+}/Zn^{2+}$ in an aqueous environment. Note that we aim to model here an isolated carboxylate group rather than specific strong binding sites made of multiple carboxylates.

Prior metal carboxylate binding constant compilations[12] and individual studies include experimental potentiometric,[13–17] NMR,[18] vibrational spectroscopic,[19–21] and surface sum frequency[22,23] measurements, as well as theoretical classical[24] and quantum[25] calculations. In the case of acetate, the range of previously reported binding constants consistently point to weak pairing with divalent cations.[12,14] However, previous works are not always in agreement regarding

the relative binding strengths of the above three cations (although studies that have included all three cations generally agree that Zn^{2+} binds more strongly to Ac^- than either Mg^{2+} or Ca^{2+}).[12,13] In addition, molecular interpretation of such binding constants remains elusive, since it is often unclear what kind of ion pairs the experiments are particularly sensitive to. On the molecular modeling side, the description of the interactions of dications with their anionic binding partners can only be as trustworthy as the underlying force field. It is, therefore, crucial to properly benchmark the interaction parameters against experimental data.[26,27]

Most prior experimental studies of metal acetate binding constants have utilized potentiometric measurements. Although such measurements have provided a vast data base of binding constant results,[94] they are inherently ambiguous with regard to the structures of the bound species, and are susceptible to systematic errors associated with interfacial electrode effects.[14,28] Vibrational spectroscopic methods offer an appealing alternative detection strategy, as the associated spectral changes contain molecularly detailed information pertaining to both the free and bound species (and their hydration shells). However, prior attempts to use vibrational infrared and Raman spectroscopy to determine metal acetate binding constants were restricted to the use of Gaussian-Lorentzian fits to the acetate CC stretch band (near 940 cm^{-1})[20,21] and did not report consistent binding constant results for Zn^{2+}, Mg^{2+} and Ca^{2+}. These prior studies also concluded that the carboxylate COO^- stretch band (near 1400 cm^{-1}) was less quantitatively useful, presumably because of its overlap with to a CH_3 deformation mode,[29] although the apparent splitting between the symmetric and antisymmetric carboxylate stretch sub-bands has been interpreted as providing some information regarding the presence of unbound (free acetate), monodentate, bidentate, and bridging complexes.[19–21]

In an effort to resolve these discrepancies, we have used a new Raman multivariate curve resolution (Raman-MCR) measurement strategy to obtain self-consistent one-to-one $Ac^-\cdots M^{2+}$ binding free energies in aqueous MAc_2 solutions (where M = Zn, Mg, or Ca). We demonstrate that a Raman-MCR based spectral decomposition strategy may be used to obtain robust metal acetate binding constants, without relying on any *a priori* assumptions regarding the shapes of the unbound and bound acetate spectra. Our results further demonstrate that self-consistent one-to-one binding constants may be obtained from aqueous MAc_2 solutions with concentrations up to 0.5 M, using spectral decompositions of either the acetate CC or COO^- bands (or both). These experimental conclusions are corroborated by our molecular dynamics (MD) simulations with a force field that effectively accounts for electronic polarization via charge scaling. Our MD results confirm that the binding affinities to the carboxylate group are not correlated with the cationic radii and also provide molecular insight into the ion pairing geometries. In particular, properly benchmarked simulations and quantum calculations allow us to address detailed structural and energetic issues concerning the modes of cation–carboxylate binding (i.e., contact vs. solvent-shared and, in the former case, monodentate vs. bidentate, see Figure 1), as deduced from spectroscopic measurements in this work as well as in previous studies.[19,20,24,29–39]
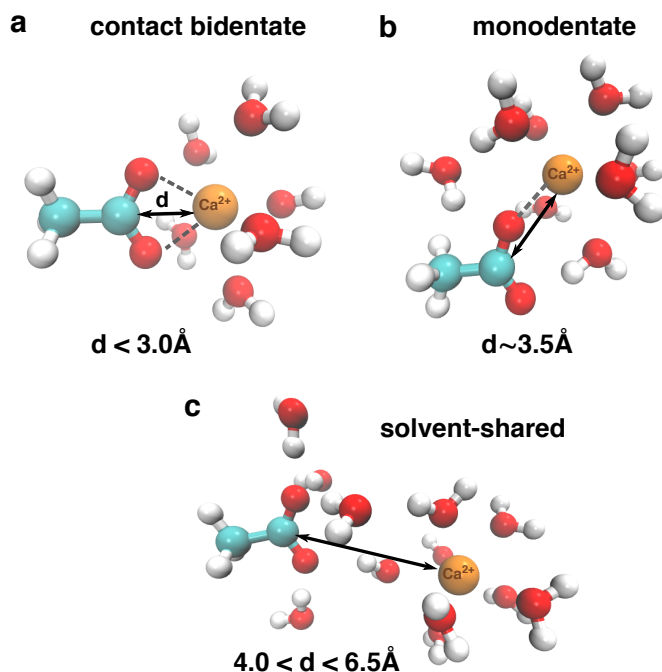
Figure 1. Sketch of the different cation-acetate ion pairing modes with the surrounding layer of water molecules, with typical associated C-cation distances (for a Ca^{2+} cation). Snapshots were prepared using the VMD software.[40]

2 Methods

2.1 Experimental details

Sample preparation and Raman-MCR spectra. Sodium acetate (Mallinkrodt, 99+%), magnesium acetate tetrahydrate (Sigma Aldrich, 99+%), calcium acetate monohydrate (Sigma Aldrich, 99+%), zinc(II) acetate dihydrate (Sigma Aldrich, 98+%), and acetic acid (Sigma Aldrich, 99.7+%) were used without further purification. Aqueous solutions of sodium acetate (NaAc), magnesium acetate ($MgAc_2$), calcium acetate ($CaAc_2$), and zinc(II) acetate ($ZnAc_2$) were prepared by adding an appropriate mass of each solid to a volumetric flask and completed with ultra-purified water (Milli-Q UF Plus, 18.2 MΩ cm, Millipore) to obtain stock solutions of 4 M (Na^+ solutions), 2 M (Mg^{2+} and Ca^{2+} solutions), or 1.5 M (Zn^{2+} solutions). Solutions were sonicated for ~1 min to aid dissolution and were then diluted to obtain the desired concentrations.

6

Raman vibrational spectra were collected at 20°C using a home-built instrument with a 514.5 nm Argon ion laser and 20 mW of power at the sample. For each sample, two to four spectra were collected with an integration time of 5 min. Raman-MCR spectra were obtained using the self-modeling curve resolution (SMCR) algorithm.[41–43] In this procedure, measured Raman spectra of pure water and solutions were decomposed to obtain minimum area non-negative solute-correlated (SC) spectra, containing vibrational features arising from the solute itself and from the water molecules that are perturbed by the solute. Unless stated otherwise, all of the reported Raman-MCR solute-correlated (SC) spectra are normalized to the solute CC band area. This normalization produces spectra whose CC band area is concentration independent, which is also the case when normalizing the SC spectra to the corresponding solute concentration. The CC normalization procedure is more effective than concentration normalization in suppressing variations due to drifts in the excitation laser intensity or optical alignment.

Ion-pairing binding constant determination. Raman-MCR SC spectra were used to determine the binding constants of acetate (Ac^-) to metal dications. For a given aqueous MAc_2 solution, the SC spectrum contains features arising from unbound Ac^-, bound Ac^-, and water molecules perturbed by these two acetate species as well as by the M^{2+} ions. Total least squares (TLS) analysis was applied to the SC spectra to estimate the concentrations of unbound Ac^- and bound Ac^-. This TLS procedure required obtaining the pure component spectra for the unbound and bound acetate species. The unbound component was chosen as the SC spectrum obtained from NaAc solutions (because the corresponding SC spectra are dominated by Ac^-, as Na^+ has a negligible influence on water structure,[44] and because there is little evidence of ion-pairing between Na^+ and Ac^- at concentrations up to 2 M, as further described in the *Results* section). The bound component, which is not readily evident in the measured SC spectra, was obtained using a second SMCR

decomposition in which the contributions of unbound Ac⁻ (aqueous NaAc) were removed from the SC spectra pertaining to each MAc$_2$ solution (as described in the Supplementary Information). The resulting second round SMCR SC spectrum obtained contains vibrational features pertaining to the bound acetate MAc⁺ species itself (as further described in the *Results* section).

For comparison of the Raman-MCR-based binding constants with previous estimates made at different ionic strengths, all values were extrapolated to zero ionic strength using the following Davies-like equation:[45,46] $\Delta \log_{10} K = \left(0.51 \frac{\sqrt{I}}{1+1.50\sqrt{I}} - 0.09I\right)\chi - 0.09I$, where I is the ionic strength, and χ is an integer that depends only on the charge and stoichiometry of the involved species ($\chi = 4$ for the dication/acetate systems).

2.2 Computational details

Molecular dynamics simulations and ΔG$_{bind}$ calculations. We used molecular dynamics simulations with different force fields to compute the binding free energy ΔG_{bind} of various cations (Ca^{2+}, Zn^{2+}, Mg^{2+}) to an acetate ion. Since sodium acetate is used experimentally as a non-binding reference, we also performed simulations with Na⁺. The simulation box contained one acetate anion, one cation (Ca^{2+}, Zn^{2+}, Mg^{2+} or Na⁺) and 1723 water molecules. The simulations were performed with the Gromacs 5.1.1 software,[47] in the constant temperature/constant pressure (NpT) ensemble, using the Parinello-Rahman barostat[48] with a 5 ps coupling time and the velocity rescaling thermostat[49] at 300 K with a 1 ps coupling time. Periodic boundary conditions were used employing a Particle Mesh Ewald[50] treatment of long-range electrostatic interactions with a 12 Å cutoff. Hydrogen-containing bonds were constrained using the LINCS algorithm,[51] and the SETTLE algorithm for water molecules.[52]

Water molecules were described by the SPC/E force field,[53] and different force fields were tested for the ions. For the cations, we first tried force fields commonly used in the literature,

including the Joung-Cheatham parameters for Na^+,[54] the $12-6$ Lennard-Jones parameters for divalent cations suggested by the Merz group,[55] the Ca^{2+} force field developed by the Netz group,[56] the Mg^{2+} force field suggested by D. Tobias and coworkers,[57] and the Zn^{2+} force field by Stote and Karplus.[58] A previously derived Amber99-like force field was employed for acetate.[26]

Standard full charge force fields are known to overestimate ion pairing, especially with divalent cations because they miss part of the charge shielding provided by solvent polarization effects. Therefore, we also tested different "scaled charge" force fields, that follow the so-called Electronic Continuum Correction (ECC) theory, which effectively takes the electronic polarization effects into account, in a mean field approach.[59-61] We tested previously developed ECC force fields for acetate[26] and for Na^+,[62] Ca^{2+},[26,63] Mg^{2+} and Zn^{2+} [27]. We also used a "milder" scaling factor of 0.8 which assumes that part of the electronic polarization is effectively wrapped into the employed empirical water model, whose dielectric constant is larger than what would correspond solely to nuclear polarization. All the employed force field parameters are provided as GROMACS parameter files as Supplementary Data.[64]

Binding free energy calculations were performed within GROMACS following the well-established double-decoupling alchemical procedure.[65-68] In a first simulation (S1), the cation in pure water is progressively decoupled from its environment (ΔG_1); in a second simulation (S2), the cation in a specific ion pair geometry with acetate is progressively decoupled from its environment (ΔG_2). This was done first turning off the electrostatic interactions between the cation and its environment, before turning off the van der Waals interactions, using soft-core potentials to improve convergence, for a total of 24 windows. Starting from the coupled state, each window was equilibrated for 250 ps before starting the next one, and another 10 ns sampling were then added in each window independently. A typical input file for one window is provided as

Supplementary Data.[64] The free energy difference associated with each alchemical transformation was reconstructed using the Bennett Acceptance Ratio[69] (BAR) method as implemented in Gromacs.[47] The error bar provided on ΔG_{bind}^{o} is the sum of the error on each free energy term ΔG_1 and ΔG_2, each being estimated from the average variance over 5 blocks as implemented by default in "gmx bar". As extensively discussed in the literature, several corrections need to be estimated to obtain the desired standard binding free energy ΔG_{bind}^{o}. First, changes in the net charge of the simulation box during ion decoupling induce a change in the neutralizing charge density, or "gellium", when using periodic boundary conditions and Particle Mesh Ewald summation. The interactions with the gellium contribute to the calculated decoupling free energies.[70–72] Analytic estimates for the correction ΔG_{PBC} have been suggested,[72] and we use here the second order expansion (Eq. 17 from Ref [72]). Second, the binding geometry of the ion pair in the simulations S2 (contact monodentate, contact bidentate, solvent-shared) was enforced by a flat-bottomed harmonic restraint on the distance between the cation and the carbon of the carboxylate group. The details of the employed restraint for each cation are provided in the Supplementary Information (Table S2). The free-energy contribution of this restraint needs to be carefully accounted for both in the coupled and the uncoupled state.[73–75] In the uncoupled state, the free energy of applying the restraint with respect to the standard state concentration can be expressed and numerically estimated as $\Delta G_{restr} = \int_0^\infty 4\pi r^2 e^{-\beta U_{restr}(r)} dr \approx \int_0^L 4\pi r^2 e^{-\beta U_{restr}(r)} dr$, where L is the box size and U_{restr} the flat-bottomed restraining potential. In practice the geometry and size of the box are irrelevant provided that $U_{restr} \gg kT$ for $r_{max} < r < L$. In the coupled state, the free energy contribution due to the removal of the restraint can be expressed as $\Delta G_{unrestr} = -kT \ln\langle e^{+\beta U_{restr}}\rangle$, numerically estimated on the fully coupled simulation window.[73] Finally, the standard binding free energy is obtained as $\Delta G_{bind}^{o} = \Delta G_1 - \Delta G_2 + \Delta G_{PBC} + \Delta G_{restr} + \Delta G_{unrestr}$. Note that the correction

term ($\Delta G_{\text{PBC}} + \Delta G_{\text{restr}} + \Delta G_{\text{unrestr}}$) is here overall of the same magnitude as the raw free energy difference, and it is thus crucial to properly take it into account. The total binding free energy for contact pairs $\Delta G_{\text{bind,tot}}^{\text{o}}$ is obtained by combining the binding free energy in each ion pair geometry, monodentate $\Delta G_{\text{bind,mono}}^{\text{o}}$ and bidentate $\Delta G_{\text{bind,bi}}^{\text{o}}$ as follows:

$$\Delta G_{\text{bind,tot}}^{\text{o}} = -RT \ \ln(e^{-\Delta G_{\text{bind,mono}}^{\text{o}}/RT} + e^{-\Delta G_{\text{bind,bi}}^{\text{o}}/RT})$$

A detailed example for one cation in one specific binding geometry is provided in the Supplementary Information.

When decoupling a cation from acetate in a monodentate binding mode, the configurational distribution of the bound state is strongly bimodal, and symmetric: it is composed of two equivalent binding modes involving each carboxylate oxygen atom. Each of these two modes is potentially metastable on the time scale of simulations, therefore the initial windows of the decoupling transformation are very likely to present incomplete sampling, unevenly distributed between the two modes. Our numerical tests indicate that this is the case with most of the full charge force fields and some scaled charge (esp. for Mg^{2+} and Zn^{2+}), however, due to the symmetry of the energy distribution, this does not introduce a bias, or even significant added variance, in our free energy estimates. See Supplementary text and Figure S4 for details.

***Ab initio* molecular dynamics simulations and free energy profiles.** We computed the free energy profiles along the distance between the carboxylate carbon atom and the different cations using Born-Oppenheimer *ab initio* molecular dynamics (AIMD) simulations, performed with the Quickstep module of the CP2K 3.0 package[76] with the hybrid Gaussian and plane waves (GPWs) method. We limited our simulations to the range of distances corresponding to the contact bidentate-monodentate ion pair conformations, because the limited sampling allowed by AIMD simulations made it impossible to converge the free energy profiles at larger distances. The

simulation box contained one cation (Ca^{2+}, Mg^{2+} or Zn^{2+}) and one formate anion (smaller than acetate for these very expensive simulations) together with 106 water molecules, the box size being determined from the average box size in NpT simulations of the same system with a classical force field. The simulations were run in the NVT ensemble at 300 K using a velocity rescaling thermostat[49] (CSVR) with a 50 fs time constant. We used the BLYP[77,78] density functional with the D3M dispersion correction[79,80] and a Becke-Johnson damping scheme,[81] D3M(BJ). The same calculations were repeated with the older D2 dispersion correction[82] to assess the robustness of the results with respect to the dispersion scheme. The electron density was described with the DZVP-MOLOPT-SR-GTH double-ζ basis set,[83] with GTH pseudopotentials[84] for the core electrons and a 400 Ry cutoff for the auxiliary plane-wave basis. We used a total of 10–15 umbrella sampling windows (depending on the cation) with the distance of interest restrained around values varying from 2.3 Å (for Mg^{2+} and Zn^{2+}) or 2.7 Å (for Ca^{2+}) to 3.75 Å. Each window was started from an equilibrated configuration obtained from a classical simulation with the same restraining potential. In the barrier region between the two binding modes, we used several starting points with different starting geometries with typical hydration patterns. We accumulated 40 ps of trajectory in each window, after a 5 ps equilibration. Each free energy profile thus aggregates around 500 ps of AIMD simulations. Free energy profiles were obtained from simulation trajectories using WHAM,[85] as implemented in ref [86]. Typical input files are provided as Supplementary Data.[64]

Raman spectra modeling. Raman spectra were modeled following a similar procedure as optimized in our previous work,[87] carefully taking into account the environment of the molecules of interest, which is essential to reach quantitative accuracy. Briefly, the surrounding water molecules are split between different regions, the closest being included in the QM region to allow for charge transfer to the cation, and the more distant ones—important for accounting for long

range electrostatic effects—treated as point charges. In order to properly sample the possible positions/orientations of water molecules and of the solutes of interest, we took 200 snapshots from the MD simulations performed in each ion pair geometry for each cation, as described for the binding free energy calculations. For each snapshot, we extracted the acetate and the bound ion, together with the water molecules that have at least one atom within 1.2 nm from either cation or acetate. The geometry of each snapshot was then optimized before calculation of the Raman spectrum. All calculations were done using the Gaussian 16 package.[88] The acetate and the bound ion were described at the B3LYP/6-31++G** level of theory, while the first layer of water molecules (any water molecule with an atom closer than 0.3 nm from any atom of acetate/cation) was described at the B3LYP/6-31G* level of theory. The water molecules in the second layer (MM region, 0.3–0.6 nm cutoff) were described using the TIP3P force field[89] and the coupling between the QM and MM regions was modeled using ONIOM method[90] with electrostatic embedding. The last layer of water molecules (0.6–~1.2 nm) was described only as partial atomic charges. Each snapshot then underwent a 10-step optimization prior spectra calculation, where the acetate, the cation, and QM layer of water molecules were allowed to move, while the second layer of water molecules and point charges remained frozen. After this optimization procedure, the vibrational frequencies and Raman intensities (SCP modulation scheme with backscattering detection (180°)) were calculated using the harmonic approximation, together with far from resonance CPKS theory[91] at 532nm. Then, the signal originating from water molecules was deleted using an in house developed script and the resulting intensities were broadened using a Lorentzian function with a full width at half maximum of 7.5 cm^{-1} and corrected for the temperature factor at 300 K.[87] The small difference between the simulation (*i.e.*, 532 nm excitation frequency and 300 K) and experimental conditions are expected to have a negligible effect on the spectra, so that both results

sets can be directly compared. Finally, the spectra of all individual snapshots were averaged to yield the final averaged Raman spectra.

3 Results

Raman spectroscopy. Figure 2A shows Raman spectra of aqueous acetic acid and sodium acetate at similar concentrations. The major peaks in these spectra arise from the solute intra-molecular CC (near 900 cm^{-1}), COO$^-$ (near 1500 cm^{-1}), and CH (near 2900 cm^{-1}) vibrational modes, as well as an OH band (near 3400 cm^{-1}) resulting primarily from water molecules. Comparison of the acetic acid and sodium acetate SC spectra reveals that deprotonation of carboxylic acid[92,93] induces a significant redshift in the CO stretch band (from ~1700 cm^{-1} for –COOH to ~1400 cm^{-1} for –COO$^-$), as well as smaller shifts in the solute CC and CH bands. The observed redshift of the acetate COO$^-$ band (relative to the acetic acid COOH band) is consistent with the fact that the extra electron is added to an antibonding orbital of the anion.[93,94] Additionally, the larger intensity of the acetate COO$^-$ band implies that the extra electron increases the corresponding polarizability derivative. Note that the acetic acid and acetate stretch CO bands overlap with smaller bands (shoulders) near 1350 cm^{-1} assigned to a CH$_3$ deformation mode.[35]
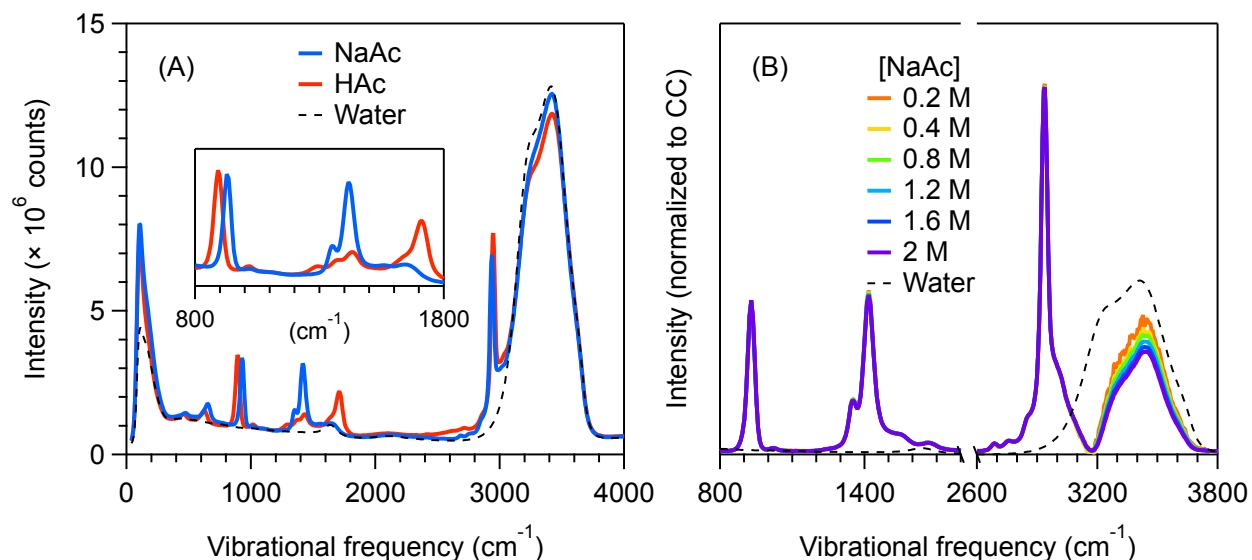
Figure 2. (A) Raman spectra of acetic acid and sodium acetate at approximately equal concentrations. (B) Raman-MCR SC spectra of sodium acetate solutions as a function of concentration. The water spectrum (dashed black) is for reference.

Figure 2B shows how the Raman-MCR SC spectra of sodium acetate vary with concentration (after normalization to the CC band area). These results indicate that there is essentially no concentration dependent shift or shape changes in the CC, COO^-, or CH bands in aqueous NaAc solutions, thus suggesting that there are no direct contacts between Na^+ and COO^- up to concentrations of ~2 M or that any direct contacts that are present do not significantly influence the acetate intramolecular vibrational modes. The only readily detectable concentration-dependent change in the aqueous NaAc Raman-MCR spectra is the slight decrease in the intensity of the NaAc Raman-MCR SC OH stretch band with increasing NaAc concentration, shown in Figure 2B. This decrease in the OH band area suggests the presence of some water-separated contacts between Na^+ and Ac^-, as would be expected to occur even in a nominally non-ion-pairing mixture of Na^+ and Ac^- at concentrations above ~1 M.

Given the negligible concentration dependence of the acetate bands in aqueous NaAc Raman spectra, the SC spectrum of NaAc may be used as a free acetate reference to uncover evidence of acetate-dication binding in aqueous of MAc_2 solutions. Specifically, Figure 3 shows that the Raman-MCR SC spectra of $MgAc_2$, $CaAc_2$, and $ZnAc_2$ solutions are shifted with respect to that of aqueous NaAc, thus implying the presence of significant ion-pairing of acetate to Mg^{2+}, Ca^{2+}, and Zn^{2+} over this concentration range. Our assignment of the shift primarily to direct (as opposed to water separated) ion paring is supported by the fact that the magnitude of the observed blue-shift of the CC stretch band is consistent with that which is predicted by quantum calculations to occur upon direct contact-ion pair formation, as further described in the *Spectra Modeling* section.
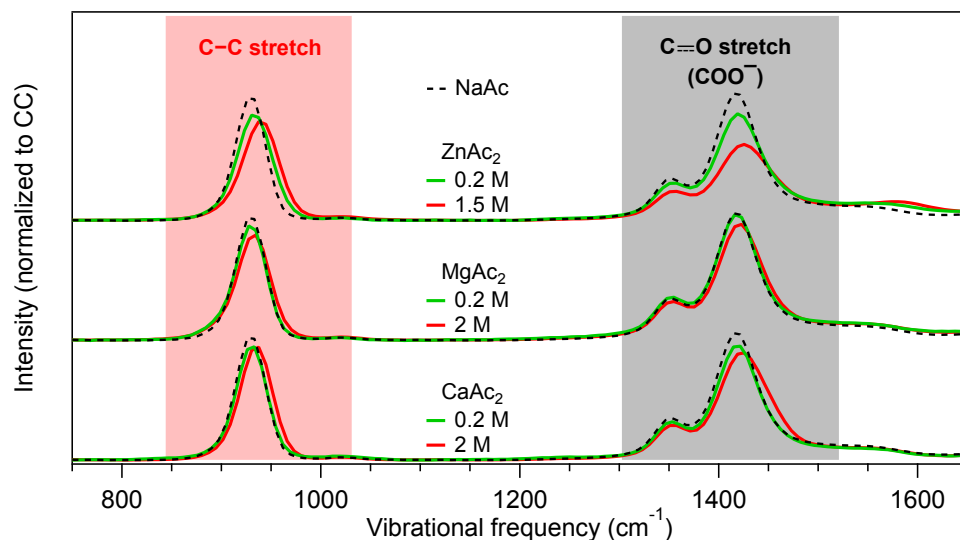

Figure 3. Concentration-dependent SC spectra of zinc(II) acetate (top), magnesium acetate (middle), and calcium acetate (bottom). The larger concentration dependent changes in the CC and COO^- stretching band intensity for $ZnAc_2$ clearly indicate that Zn^{2+} interacts more strongly with Ac^- than either Ca^{2+} or Mg^{2+}. The dashed black spectrum corresponds to aqueous sodium acetate and is included as reference for the unbound acetate spectrum. The spectra are vertically offset for clarity.

The results in Figure 3 further suggest that direct-contact ion-pairing of acetate to Zn^{2+} produces a larger spectral change than binding to either Ca^{2+} or Mg^{2+}, as evidenced by the larger concentration-dependent changes in the SC spectra of $ZnAc_2$ than either $MgAc_2$ and $CaAc_2$ at the same concentration. A quantitative experimental estimate of the corresponding binding constants can, in principle, be obtained by decomposing the measured spectra into a linear combination of the unbound and bound acetate spectra. This procedure requires knowing *a priori* the SC spectra of these two pure component acetate species. The spectrum of aqueous NaAc yields the unbound COO^- SC spectrum (as previously discussed). The spectrum of the bound acetate species is more difficult to unambiguously determine. However, we have found that a self-consistent estimate of this spectrum may be obtained using a second round SMCR procedure in which the contribution of unbound acetate (obtained from the aqueous SC spectrum of NaAc) is removed from the SC spectra of aqueous MAc_2 solutions (as further described in the Supplementary Information). Briefly, the second round SMCR analysis produces a family of possible bound spectra, but only one member of this family is found to produce a self-consistent (concentration-independent) one-to-one binding constant over the experimental concentration range of 0.1 M to 0.5 M MAc_2. The remaining members of the family of possible bound spectra include a mathematical lower bound minimum area spectrum (pertaining to the most tightly bound ion-pairs with the smallest possible binding constant), as well as a distribution of other possible bound spectra whose shape approaches that of the free acetate (pertaining to the most loosely bound ion-pairs with the largest binding constants). Although all of these bound spectra are mathematically possible, only one yields the self-consistent one-to-one binding constants between acetate and each of the three cations. The robustness of the resulting binding constant is confirmed by very similar results obtained when performing the TLS spectral decomposition using only the CC or COO^- bands or by

17

simultaneously fitting both bands (as further discussed below and in the Supplementary Information).

Figure 4A-C shows the free (dashed black) and bound (dashed red) acetate spectra, obtained as described above (and in the Supplementary Information), and the corresponding quantitative decomposition of the aqueous MAc_2 solution spectra, along with the measured SC spectrum for an aqueous 0.5 M MAc_2 solution (green curve). The inset spectra on the right-hand panels show the essentially perfect agreement between the TLS reconstructions (dotted black curves) and the measured 0.5 M SC spectra (solid green curves), where the TLS spectra represent a best-fit of the measured spectrum to a linear combination of the unbound and bound spectra. The yellow points in the right-hand panels in Figure 4 show the resulting bound acetate fraction obtained for solutions with MAc_2 concentrations up to 0.5 M, and thus total acetate concentrations up to 1 M. Note that these binding constants imply that Zn^{2+} has a binding constant to acetate ($K = 4.5 \pm 1.3$) that is about four times larger than Mg^{2+} ($K = 1.1 \pm 0.4$) and Ca^{2+} ($K = 1.1 \pm 0.4$). The experimental points (Figure 4 D-E-F) are well fitted with a single 1:1 binding constant, which strongly suggests that no significant 2:1 binding occurs in this range of concentrations, in agreement with earlier ultrasonic absorption experiments.[95]
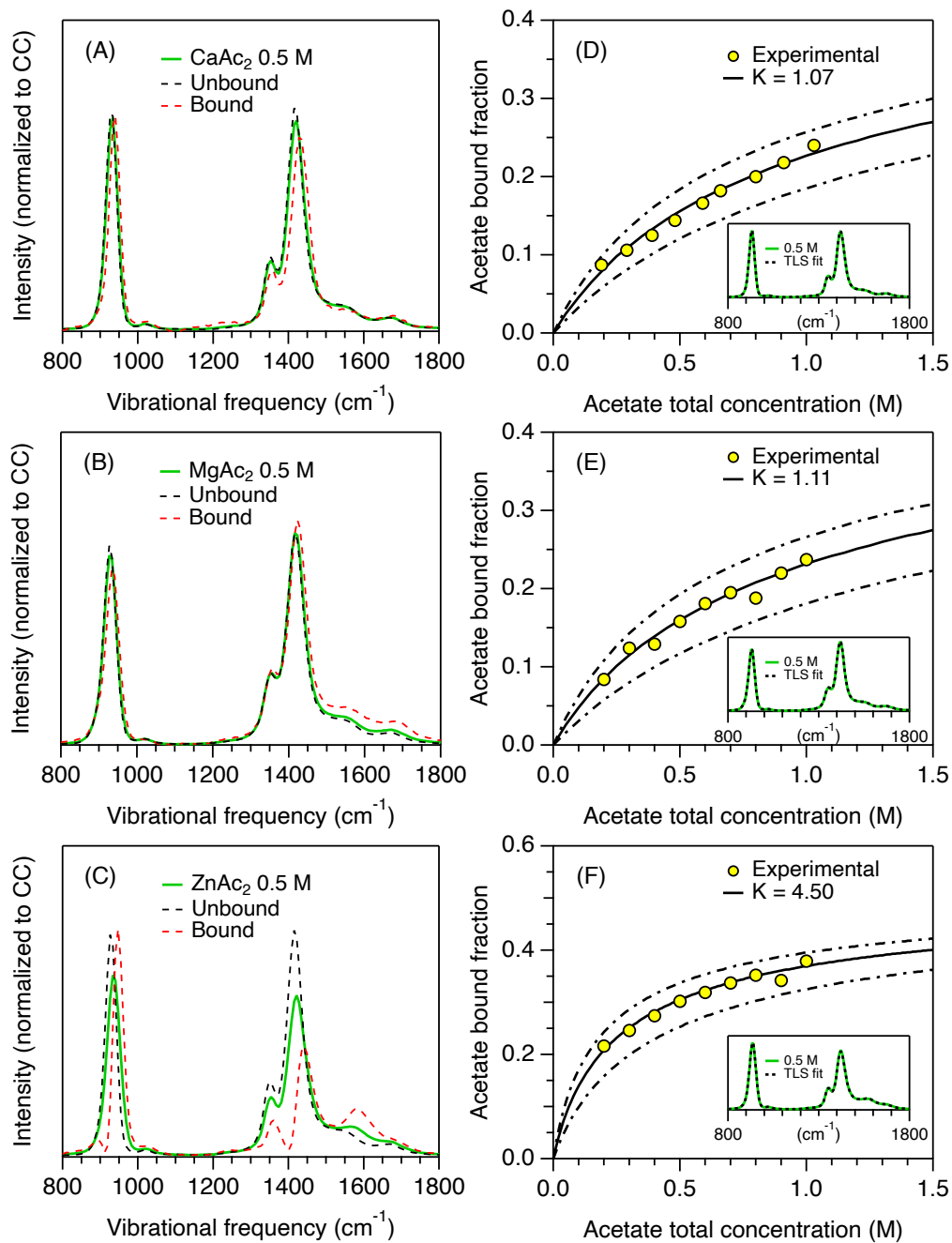
Figure 4. Free and bound component spectra (left-hand panels A–C) and binding curves (right-hand panels D–F) for magnesium (A and D), calcium (B and E) and zinc (C and F). The inset spectra in panels D–F compare the TLS reconstruction (dotted black curves) with the experimental SC spectrum (solid green curves) obtained for a 0.5 M solution of MAc_2. The dot-dashed curves represent a 99% confidence interval for the binding constants.

Spectra modeling. While the previously described Raman experiments provide an experimental measure of the binding constant between divalent cations and acetate, they cannot determine the geometry of the observed ion pairs and have a quite limited ability to distinguish different types of ion pairs: contact monodentate, contact bidentate or solvent shared ion pairs. In order to determine which type of ion pairs can lead to a shift in the measured Raman spectra, we computed the spectra (Figure 5) of acetate involved in different ion pair configurations with Ca^{2+}, Mg^{2+}, Zn^{2+}, and Na^+ using quantum chemical (DFT-based) calculations on a large number of snapshots extracted from molecular dynamics simulations (see Methods). Although the shape of the band near ~1450 cm^{-1} is not perfectly reproduced, both peaks (~950 cm^{-1} and ~1450 cm^{-1}) exhibit a blue shift when in contact ion pair with Ca^{2+}, Mg^{2+}, and Zn^{2+}. This is more pronounced for the bidentate ion pair and for Zn^{2+} and Mg^{2+} than Ca^{2+}, which is in very good agreement with the experiment, and thus validates the procedure used to extract the signal of the bound acetate from the raw spectra.

The first important finding is that the simulated spectra show that no significant shift is observed between the reference spectrum of acetate in pure water, and that of acetate ion paired with Na^+ (see Supplementary Information). This validates the use of the sodium acetate solution as the "unbound" reference in the experiment. It also shows that even if there was significant pairing between acetate and sodium cations, the Raman experiment would not be able to capture it. The computed spectra for the contact ion pairs with Ca^{2+}, Mg^{2+}, and Zn^{2+} exhibit a blue-shift in the CC stretch band (near 940 cm^{-1}) that is more pronounced for Zn^{2+} and Mg^{2+} than Ca^{2+} and are larger for the bidentate than the monodentate ion pairs. It is also clear that the formation of solvent-shared ion pairs (for all cations) does not significantly affect the peak positions. Hence, the experimental binding-induced spectral changes are evidently due primarily to the formation of

20

direct contact ion pairs. The fact that the predicted $Zn^{2+}\cdots Ac^-$ bidentate shift of ~30 cm^{-1} is comparable to the experimentally observed shift of ~20 cm^{-1} suggests that the experimental $ZnAc_2$ solutions may include bidentate bound species (over the experimental concentration range up to 0.5M), probably in addition to monodentate ones. In contrast, the smaller experimental binding-induced CC band shifts of ~10 cm^{-1} for Mg^{2+} may imply that the binding is primarily monodentate over the experimental concentration range. For Ca^{2+}, the calculated shifts for bidentate and monodentate ion pairs are much more similar, so that no clear conclusion regarding the contact ion pair structure can be drawn.
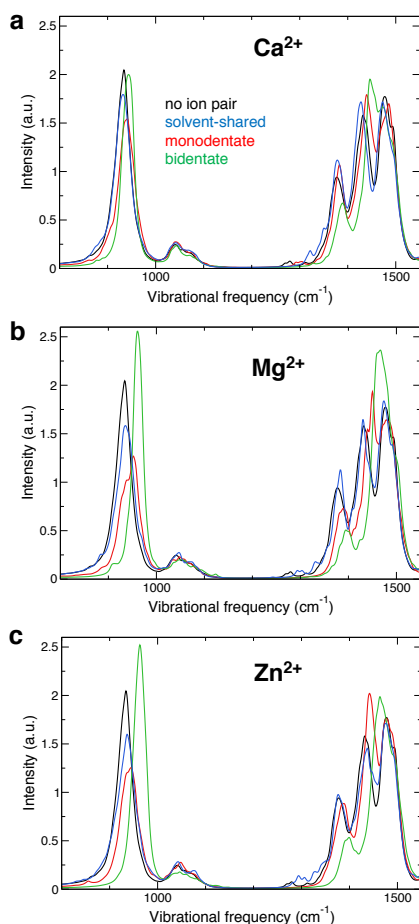

Figure 5. Simulated Raman spectra for acetate in pure water (black) or involved in a contact monodentate (red), contact bidentate (green) or solvent-shared (blue) ion pair with a a) calcium, b) magnesium and c) zinc cation.

Binding constants and ion pair geometries. Since Raman measurements are primarily sensitive to direct contact ion pairs, they cannot assess the relative stability of contact vs solvent shared ion pairs or provide detailed information about the preferential mode of binding (monodentate or bidentate). Hence, molecular dynamics simulations can help complement the picture by providing access to the molecular details of the interaction and assess the relative stability of different ion pair structures.

However, standard nonpolarizable force fields are known to suffer from severe over-binding artefacts to describe the interaction between divalent cations and negatively charged moieties.[26,96] These artefacts essentially originate from the lack of electronic polarization in such force fields. Several schemes have been suggested to correct this limitation, either through explicit inclusion of electronic polarization with the development of fully polarizable force fields (e.g. [73,97–100]), or through a mean-field approach, the Electronic Continuum Correction,[59–61,63] that suggests to implicitly account for electronic polarization by scaling the charge of charged moieties by a factor of $1/\sqrt{\varepsilon_{el}} = 0.75$, where $\varepsilon_{el} = 1.78$ is the electronic part of the water dielectric constant. A milder factor 0.8 has also been tested as an attempt to compensate the fact water models have a dielectric constant that already contains more than pure nuclear polarization (see Methods). In a first step, we thus assessed the quality of different force fields—nonpolarizable with either full or scaled charges, and polarizable, with the AMOEBA force field[97]— against the experimentally determined binding constants. Table 1 summarizes the obtained results, showing the range of binding free energy values in the cases where several force fields were tested. The uncertainty on each value is on the order of 0.5 kJ mol^{-1}, and the details of the tested force fields and associated binding free energies are provided in the Supplementary Information (Table S4-S7).

It is important to notice that the Raman-derived binding constants for the contact ion pairs (or equivalently binding free energies) are obtained at finite ionic strength (between ~0.3 and ~1.5 M), while calculated binding free energies correspond to a standard binding free energy in the infinite dilution limit. Hence, to compare measured and calculated binding free energies, we first extrapolated the experimentally-derived binding free energies to zero ionic strength, using a refined Davies[45,46]-like equation fitted on a large set of ion-ion binding constants measured at different ionic strengths.[46] We thus report in Table 1 the extrapolated experimental binding free energy, which can be directly compared with the computed contact binding free energy, that encompasses both monodentate and bidentate binding geometries. Note that these extrapolated binding free energies are still quite small, around -3.2 kJ mol^{-1} for Ca^{2+}, -3.4 kJ mol^{-1} for Mg^{2+}, and only -6.9 kJ mol^{-1} for Zn^{2+}.

Table 1. Standard binding free energy of different divalent cations with acetate at zero ionic strength as extrapolated from the Raman experiments, and calculated for different ion pair geometries using either a full charge force field, an ECC force field with the usual 0.75 scaling factor or with a 0.8 scaling factor, and with the fully polarizable AMOEBA force field. The details of the employed force fields and corresponding binding free energies are provided in the Methods section and Supplementary Information (Sections 2 and 3, Tables S4-S7). When different force fields were tested, the two values are separated with /. The error bar on all calculated values is about 0.5 kJ mol^{-1}.

$\Delta G_{bind}°$ (kJ mol^{-1})	Experimental ($I = 0$)	Full charge FF	ECC FF (scaling 0.75)	ECC FF (scaling 0.8)	AMOEBA
Ca^{2+}					
Contact bidentate	n.a.	$-12.3 / -21.7$	$+5.4 / +6.3$	$+2.5$	-2.0
Contact monodentate	n.a.	$-10.1 / -18.4$	$+2.0 / -0.6$	0.0	-11.3
Total contact	***-3.2 ± 0.2***	***$-13.2 / -22.3$***	***$+1.5 / -0.7$***	***-0.8***	***-11.4***
Solvent-shared	n.a.	-6.7	$-2.5 / -3.1$	-2.7	-1.7
Mg^{2+}					

Contact bidentate	n.a.	−29.9 / −13.0	+18.1 / +19.7	+15.6	n.a.
Contact monodentate	n.a.	−34.1 / −37.4	−0.6 / −0.1	−5.3	−11.9
Total contact	***−3.4 ± 0.4***	***−34.5 / −37.4***	***−0.6 / −0.1***	***−5.3***	***−11.9***
Solvent-shared	n.a.	−6.6 / −6.8	−3.4 / −1.1	−1.3	−1.8
Zn^{2+}					
Contact bidentate	n.a.	−14.9	+21.4	+19.4	n.a.
Contact monodentate	n.a.	−36.8	+0.6	−3.7	n.a.
Total contact	***−6.9 ± 0.4***	***−36.8***	***+0.6***	***−3.7***	n.a.
Solvent-shared	n.a.	−6.9	−2.0	−2.4	n.a.

The binding free energy calculations show that nonpolarizable full charge force fields strongly overestimate the strength of the cation-acetate interaction, by at least 10 kJ mol^{-1} for Ca^{2+}, and by about 30 kJ mol^{-1} for Mg^{2+} and Zn^{2+}, and thus cannot be trusted to give a faithful representation of these binding processes. In contrast, ECC force fields with the standard 0.75 scaling factor predict much weaker binding constants, qualitatively in better agreement with the experiment, notably for Mg^{2+} and Zn^{2+}, but quantitatively too weak by about 3–4 kJ mol^{-1}. Since several works[101,102] suggested that the use of a water force field that does not have the expected dielectric constant would justify using a scaling factor larger than 0.75 (but always smaller than 1), we performed simulations with test versions of the acetate and cation force fields using a scaling factor of 0.8. This indeed in all cases improved the predicted binding free energy. However, the difference between the binding free energies for Ca^{2+} and Mg^{2+} is too large in the simulations (they are identical within error bars in the experiment), and none of the force fields describes the significantly stronger (by 3.5 kJ mol^{-1}) binding with Zn^{2+} compared to the two other cations. For comparison, we also computed for Ca^{2+} and Mg^{2+} the binding free energy to acetate using the AMOEBA fully polarizable force field, which seems to overestimate the binding strength by about

8 kJ mol^{-1} for both cations. However, it does capture the almost identical binding constants of the two cations with acetate, which nonpolarizable force fields do not properly reproduce. Hence, even if the polarizable description still constitutes for Mg^{2+} a big improvement over full charge nonpolarizable force fields, the results are not in quantitative agreement with experimental data.

4 Discussion

Comparison with earlier experimental estimates of K. Several estimates of the cation-acetate binding constants are available in the literature and can be compared to the presently obtained results (Table 2). Since the simulations effectively pertain to the zero ionic strength limit, we extrapolated all the values to zero ionic strength using a refined Davies-like equation[46] (if the extrapolation was not already performed in the original work). Note that previous data have been obtained with potentiometric measurements, with older reported data potentially suffering from the lack of correction for liquid junction potentials.[14,28] In addition, while we have shown that the present Raman-derived binding constants mainly report on the formation of contact ion pair, it is not clear how sensitive the potentiometric measurements are with respect to different ion pair geometries, even if one would expect it to be also mostly, but probably not exclusively, sensitive to contact ion pairs. Keeping these remarks in mind, our results show that Zn^{2+} binds about four times more strongly to acetate than either Ca^{2+} or Mg^{2+}, in qualitative agreement with previous potentiometric measurements[12,13] (and better quantitative agreement with more recently corrected potentiometric results[14] for acetate binding to Ca^{2+}). The difference between the binding constants of Ca^{2+} and Mg^{2+} is small and lies within the experimental error bars. This is in line with all previous studies that reported very similar binding constants for the two cations, either slightly in favor of one or the other, the difference probably being in each case within experimental error.

Table 2. Comparison of the standard binding constant $K°$ at zero ionic strength for the formation of the 1:1 cation:acetate complex for different divalent cations, as obtained from present Raman experiments and from previous studies, all of which being extrapolated to zero ionic strength as described in ref [46].

	Present work	Ref [13]	Ref [12]	Ref [17]	Ref[14]
Ca^{2+}	3.6 +/− 0.4	11.0	15.4 +/− 1.1	10.4	2.7 +/− 0.3
Mg^{2+}	3.9 +/− 0.6	10.3	18.6 +/− 1.0	9.5	n.a.
Zn^{2+}	16.0 +/− 2.8	28.3	37.2	n.a.	n.a.

Lessons learnt for ion pairing simulations. Comparing experimental binding estimates for the formation of ion pairs and values obtained with different force fields clearly highlighted the need to include electronic polarization to obtain a qualitatively correct picture, confirming previous studies.[26,96] Standard nonpolarizable force fields systematically strongly overestimate the binding strength, by sometimes as much as 30 kJ mol^{-1}, the error being more dramatic with small divalent ions such as magnesium and zinc. While explicit treatments of electronic polarization in force fields should be in principle better than the implicit mean-field charge scaling treatment used in the ECC approach, our results show that the former methods, at least in their current versions, do not always lead to better predictions than the ECC treatment. In some cases, such as the Mg^{2+}–acetate binding, the tested explicitly polarizable force field even performs significantly worse, even if it accurately predicts the same binding strength for calcium and magnesium. Hence, each force field should be thoroughly tested for the system and quantity of interest, with no guarantee that more elaborate force fields, in their current development state, provide more accurate results. Interestingly, for the ECC force field, in all the cases reported here, a 0.8 scaling performs significantly better than the standard "physically-sound" 0.75 scaling prescribed by the ECC

theory. While this had been suggested before[101] and can be rationalized in terms of limits of the available water models, this issue will be further investigated in future works.

Insights into binding patterns. Since our simulated spectra showed that the Raman experiments report mostly the formation of contact ion pairs, the present experiments demonstrate the existence of contact ion pairs between acetate and all the studied divalent cations. Even if the ratio between contact and solvent-shared ion pairs remains out of reach experimentally, our experimental and theoretical results imply that there is significant direct contact ion pair formation between acetate and the three dications (Mg^{2+}, Ca^{2+}, and $Zn^{2+)}$ in aqueous MAc_2 solution with concentrations down to 0.1 M. This conclusion is inconsistent with the assumption that some of these dications, such as Mg^{2+}, always retains its hydration shell when ion-pairing with COO^-.

In addition, our free energy calculations allow us to estimate the relative contact/solvent-shared binding, but the picture strongly depends on the details of the employed force field. For instance, while the AMOEBA polarizable force field predicts a very strong preference for the contact ion pairs with calcium, both ECC force fields predict the solvent-shared ion paired to be slightly more favorable, none of them quantitatively capturing the binding free energy. With the magnesium cation, both the 0.8-scaling ECC (in quantitative agreement with the experiment for the binding free energy) and the AMOEBA force fields exhibit a preference for the contact binding, even if the ratio (or equivalently, the free energy difference) with the solvent-shared geometry is quite different (larger with AMOEBA). Since none of the force fields captures the stronger binding with Zn^{2+} compared to the other cations, probably due to a missing partly covalent contribution, the details of its binding behavior can probably not be trusted in any classical simulation.

Another controversial point in the literature is the nature of the favored contact binding mode for the different cations: monodentate (cation in direct contact with only one oxygen of the

carboxylate group) or bidentate (cation in contact with both oxygen atoms).[24,30,34,36,103,104] For Mg^{2+}, all tested force fields, including the polarizable AMOEBA force field, give a consistent picture of the monodentate geometry being strongly favored. This is in agreement with the insights obtained from the comparison between measured and modeled spectral shifts (see *Results* section) and with several earlier reports,[30,34,103,104] but conflicting with a previous study by some of us that suggested monodentate and bidentate modes to be both existing in solution.[24] All force fields provide the same picture for Zn^{2+} as for Mg^{2+}, with exclusive monodentate binding, but since they do not capture the specificity of zinc binding, they cannot be trusted to correctly describe binding modes. For Ca^{2+}, the picture provided by the simulations is much less clear. While some force fields (incl. AMOEBA) predict the almost exclusive existence of the monodentate binding mode, others (incl. ECC with 0.8 scaling) predict an equilibrium between the two forms, even if the monodentate binding is always slightly favored. These findings are qualitatively consistent with earlier studies that suggested that Ca^{2+} slightly favored monodentate over bidentate binding,[36,104] but that it was more prone to bidentate binding than Mg^{2+}.[30,104]

To complement the picture provided by classical force field simulations—not always very conclusive especially for Zn^{2+} and Ca^{2+}—we performed DFT-based *ab initio* molecular dynamics simulations on small systems, using formate instead of acetate due to the large computational cost of such simulations (see Methods). We obtained for each cation the free energy profile (Figure 6) along the distance between the carboxylate carbon atom and the cation, in the region corresponding to the bidentate (short distances) to monodentate (larger distances) transformation. Due to the limited sampling allowed by these very expensive simulations, the error bar on the free energy profile is quite large, and difficult to estimate precisely, on the order of 4–5 kJ mol^{-1}. However, the simulations are found robust to details of the simulation setup (in particular the dispersion

correction, see Supplementary Information Fig. S5) and still bring very informative insight. Indeed, our AIMD simulations confirm that Mg^{2+}–acetate ion pairs are only stable in a monodentate geometry (C–Mg distance of 3.1 Å), the bidentate ion pair being more than 25 kJ mol^{-1} higher in free energy. In contrast, both geometries appear possible and as probable (within the error bars) with Ca^{2+}, again qualitatively confirming the picture from ECC force fields and previous AIMD simulations,[26,105] but in contrast with the AMOEBA picture of exclusive monodentate pairing. For Zn^{2+}, the AIMD simulations are in line with previous suggestions in the literature that the monodentate and bidentate binding modes are of similar stability, in contrast with what is predicted by all tested force fields, but in line with our comparison between measured and computed spectral shifts (see *Results* section).
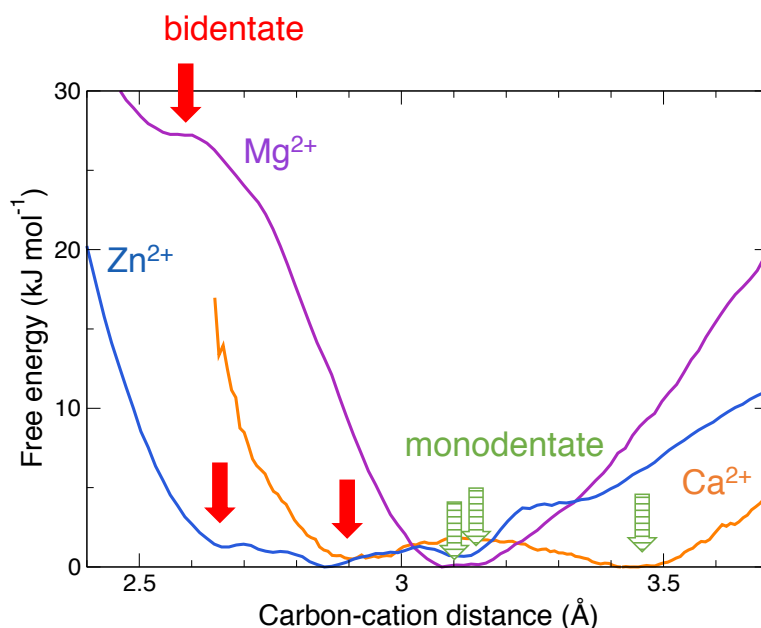

Figure 6. Free energy profiles along the carboxylate carbon-cation distance for calcium (orange), magnesium (purple) and zinc (blue) as obtained from DFT-based *ab initio* MD simulations. The location of the bidentate and monodentate ion pairs is indicated with red and dashed green arrows, respectively. No correction for the effective volume difference between the monodentate and bidentate structure has been done, because of the difficulty to estimate it properly given our limited sampling, but the largest expected

correction, $-RT\ln2 = -1.7$ kJ/mol in favor of the monodentate binding mode is well below the actual error bars of our simulation (4–5 kJ/mol)

5 Conclusion

In this study, we quantified binding of Zn^{2+}, Ca^{2+}, and Mg^{2+} to acetate anions using a combination of Raman-MCR spectroscopic measurements and both quantum and classical calculations, including molecular dynamics simulations with a force field that accounts for electronic polarization in a mean-field way via charge scaling. The Raman-MCR measurements yield self-consistent bound spectra and one-to-one binding constants demonstrating that Zn^{2+} binds about four times more strongly to acetate than either Ca^{2+} or Mg^{2+}, in qualitative agreement with previous potentiometric measurements[12,13] (and better quantitative agreement with more recently corrected potentiometric results[14] for acetate binding to Ca^{2+}). Results from the present molecular dynamics simulations agree semi-quantitatively with the Raman experimental data. Our simulations and quantum calculations further confirm that the Raman-MCR measurements are primarily sensitive to direct contact, as opposed to water-separated, ion pairing between the dications and the COO^- group, and suggest that the experimentally detected bound species may include both monodentate and bidentate binding to Zn^{2+}, but primarily monodentate binding to Mg^{2+} (over the experimental concentration range). Our results clearly demonstrate that the binding of acetate to these three cations does not scale with cation size, as both Zn^{2+} and Mg^{2+} are about 25% smaller than Ca^{2+}.[106] The observed binding constants also do not scale with ion polarizability, as Zn^{2+} and Ca^{2+} are about twice as polarizable as Mg^{2+}.[107] The more favorable binding of acetate to Zn^{2+} may perhaps be related to its higher electron binding affinity than either Mg^{2+} or Ca^{2+} (as inferred from the corresponding second ionization potentials),[108] and perhaps also to the fact that the valence electrons of Zn^{2+} are in d-orbitals while those of Mg^{2+} and Ca^{2+} are in p-orbitals.

Our combined experimental and theoretical results demonstrate both the promise and outstanding challenges associated with quantifying non-covalent ion-paring interactions in aqueous solutions. The stronger acetate binding of Zn^{2+} than either Mg^{2+} or Ca^{2+} undoubtedly has biological implications to such processes as calcium signaling, stabilization of nucleic acids by magnesium, and zinc-mediated enzymatic activity. Our results also highlight the challenges associated with quantitatively linking experimental and theoretical ion-pairing results, including the need for improved cation force fields and improved procedures for resolving the range of ion-paired structures detected using different experimental methods.

References

1. Brini, M., Ottolini, D., Cali, T. & Carafoli, E. *Calcium in health and disease. Metal ions in life sciences*, Springer Science+Business Media, 2013. vol. 13.

2.   Clapham, D. E. Calcium Signaling. *Cell*, 2007, **131**, 1047–1058.

3.   Yamanaka, R., Shindo, Y. & Oka, K. Magnesium Is a Key Player in Neuronal Maturation and Neuropathology. *Int. J. Mol. Sci.*, 2019, **20**, 3439.

4.   Romani, A. M. P. Magnesium in Health and Disease. in *Interrelations between Essential Metal Ions and Human Diseases,* Springer Science+Business Media Dordrecht, 2013. (eds. Sigel, A., Sigel, H. & Sigel, R. K.) 49–79 doi:10.1007/978-94-007-7500-8.

5.   de Baaij, J. H. F., Hoenderop, J. G. J. & Bindels, R. J. M. Magnesium in man: Implications for health and disease. *Physiol. Rev.*, 2015, **95**, 1–46.

6.   Coleman, J. E. Zinc Proteins : Enzymes , Storage Replication Proteins. *Annu. Rev. Biochem.*, 1992, **61**, 897–946.

7.   Frassinetti, S., Bronzetti, G. L., Caltavuturo, L., Cini, M. & Croce, C. Della. The Role of Zinc in Life: A Review. *J. Environ. Pathol. Toxicol. Oncol.*, 2006, **25**, 597–610.

8.   Gifford, J. L., Walsh, M. P. & Vogel, H. J. Structures and metal-ion-binding properties of the Ca2+-binding helix-loop-helix EF-hand motifs. *Biochem. J.*, 2007, **405**, 199–221.

9.   Klug, A. & Schwabe, J. W. Zinc fingers. *FASEB J.*, 1995, **9**, 597–604.

10.   Hsiao, C. & Williams, L. D. A recurrent magnesium-binding motif provides a framework for the ribosomal peptidyl transferase center. *Nucleic Acids Res.*, 2009, **37**, 3134–3142.

11.   Mason, P. E., Jungwirth, P. & Duboué-Dijon, E. Quantifying the Strength of a Salt Bridge by Neutron Scattering and Molecular Dynamics. *J. Phys. Chem. Lett.*, 2019, **10**, 3254–3259.

12.   Martell, A. E. & Smith, R. M. *Critical Stability Constants 3: other organic ligands*. 1977. doi:10.1007/978-1-4757-1568-2.

13.   Bunting, J. & Thong, K. M. Stability constants for some 1:1 metal carboxylate complexes. *Can. J. Chem.*, 1970, **48**, 1654.

14.   Stumpff, F. & McGuigan, J. A. S. Measuring Ca2+ binding to short chain fatty acids and gluconate with a Ca2+ electrode: Role of the reference electrode. *Anal. Biochem.*, 2014, **459**, 46–52.

15.   Bretti, C., Majlesi, K., De Stefano, C. & Sammartano, S. Thermodynamic Study on the Protonation and Complexation of GLDA with Ca2+ and Mg2+ at Different Ionic Strengths and Ionic Media at 298.15 K. *J. Chem. Eng. Data*, 2016, **61**, 1895–1903.

16.   McGuigan, J. A. S., Kay, J. W. & Elder, H. Y. Ionised concentrations in calcium and magnesium buffers: Standards and precise measurement are mandatory. *Prog. Biophys.*

Mol. Biol., 2016, **121**, 195–211.

17.   Emara, M., Farid, A. & Wasfi, A. Thermodynamics of Ionic Association in Aqueous Solutions of Ca and Mg organic salts using ion-selective electrode technique. *Electrochim. Acta*, 1980, **26**, 1705–1708.

18.   Wallace, M., Hicks, T., Khimyak, Y. Z. & Angulo, J. Self-Correcting Method for the Measurement of Free Calcium and Magnesium Concentrations by 1H NMR. *Anal. Chem.*, 2019, **91**, 14442–14450.

19.   Tackett, J. E. FT-IR characterization of metal acetates in aqueous solution. *Appl. Spectrosc.*, 1989, **43**, 483–489.

20.   Quilès, F. & Burneau, A. Infrared and Raman spectra of alkaline-earth and copper(II) / acetates in aqueous solutions. *Vib. Spectrosc.*, 1998, **16**, 105–117.

21.   Rudolph, W. W. & Irmer, G. A Raman Spectroscopic Study of Aqueous La(CH3CO2)3 Solutions and La(CH3CO2)3·1.5 H2O(cr). *J. Solution Chem.*, 2017, **46**, 190–214.

22.   Tang, C. Y., Huang, Z. & Allen, H. C. Binding of Mg2+ and Ca2+ to Palmitic Acid and Deprotonation of the COOH Headgroup Studied by Vibrational Sum Frequency Generation Spectroscopy. *J. Phys. Chem. B*, 2010, **114**, 17068–17076.

23.   Denton, J. K. *et al.* Molecular-level origin of the carboxylate head group response to divalent metal ion complexation at the air–water interface. *Proc. Natl. Acad. Sci.*, 2019, **116**, 14874–14880.

24.   Wahab, A. *et al.* Ultrasonic velocities, densities, viscosities, electrical conductivities, raman spectra, and molecular dynamics simulations of aqueous solutions of Mg(OAc)2 and Mg(NO3)2: Hofmeister effects and ion pair formation. *J. Phys. Chem. B*, 2005, **109**, 24108–24120.

25.   Mehandzhiyski, A. Y., Riccardi, E., van Erp, T. S., Trinh, T. T. & Grimes, B. A. Ab Initio Molecular Dynamics Study on the Interactions between Carboxylate Ions and Metal Ions in Water. *J. Phys. Chem. B*, 2015, **119**, 10710–10719.

26.   Martinek, T. *et al.* Calcium ions in aqueous solutions: Accurate force field description aided by ab initio molecular dynamics and neutron scattering. *J. Chem. Phys.*, 2018, **148**, 222813.

27.   Duboué-Dijon, E., Mason, P. E., Fischer, H. E. & Jungwirth, P. Hydration and Ion Pairing in Aqueous Mg2+ and Zn2+ Solutions: Force Field Description Aided by Neutron Scattering Experiments and Ab Initio Molecular Dynamics Simulations. *J. Phys. Chem. B*,

2017, **122**, 3296–3306.

28. Marcus, Y. & Hefter, G. Ion pairing. *Chem. Rev.*, 2006, **106**, 4585–4621.

29. Caminiti, R., Cucca, P., Monduzzi, M., Saba, G. & Crisponi, G. Divalent metal-acetate complexes in concentrated aqueous solutions. An X-ray diffraction and NMR spectroscopy study. *J. Chem. Phys.*, 1984, **81**, 543–551.

30. Dudev, T. & Lim, C. Principles governing Mg, Ca, and Zn binding and selectivity in proteins. *Chem. Rev.*, 2003, **103**, 773–787.

31. Dudev, T. & Lim, C. Effect of Carboxylate-Binding Mode on Metal Binding / Selectivity. *Acc Chem Res*, 2007, **40**, 53–56.

32. Ryde, U. Carboxylate Binding Modes in Zinc Proteins: A Theoretical Study. *Biophys. J.*, 1999, **77**, 2777–2787.

33. Paterova, J. *et al.* Microhydration of the magnesium(II) acetate cation in the gas phase. *J. Phys. Chem. A*, 2011, **115**, 6813–6819.

34. Semmler, J., Irish, D. E. & Ozeki, T. Vibrational spectral studies of solutions at elevated temperatures and pressures. 12. Magnesium acetate. *Geochim. Cosmochim. Acta*, 1990, **54**, 947–954.

35. Wang, L. Y., Zhang, Y. H. & Zhao, L. J. Raman spectroscopic studies on single supersaturated droplets of sodium and magnesium acetate. *J. Phys. Chem. A*, 2005, **109**, 609–614.

36. Einspahr, H. & Bugg, C. E. The geometry of calcium carboxylate interactions in crystalline complexes. *Acta Crystallogr. Sect. B Struct. Crystallogr. Cryst. Chem.*, 1981, **37**, 1044–1052.

37. Yang, M. M., Crerar, D. A. & Irish, D. E. A Raman spectroscopic study of lead and zinc acetate complexes in hydrothermal solutions. *Geochim. Cosmochim. Acta*, 1989, **53**, 319–326.

38. Katz, A. K., Glusker, J. P., Markham, G. D. & Bock, C. W. Deprotonation of water in the presence of carboxylate and magnesium ions. *J. Phys. Chem. B*, 1998, **102**, 6342–6350.

39. Dudev, T. & Lim, C. Monodentate versus Bidentate Carboxylate Binding in Magnesium and Calcium Proteins: What Are the Basic Principles? *J. Phys. Chem. B*, 2004, **108**, 4546–4557.

40. Humphrey, W., Dalke, A. and Schulten, K. VMD - Visual Molecular Dynamics. *J. Molec.*

Graph., 1996, **14**, 33–38.

41. Davis, J. G., Gierszal, K. P., Wang, P. & Ben-Amotz, D. Water structural transformation at molecular hydrophobic interfaces. *Nature*, 2012, **491**, 582–5.

42. Gierszal, K. P. *et al.* Π-Hydrogen Bonding in Liquid Water. *J. Phys. Chem. Lett.*, 2011, **2**, 2930–2933.

43. Lawton, W. H. & Sylvestre, E. A. Self Modeling Curve Resolution. *Technometrics*, 1971, **13**, 617–633.

44. Perera, P. N., Browder, B. & Ben-Amotz, D. Perturbations of water by alkali halide ions measured using multivariate raman curve resolution. *J. Phys. Chem. B*, 2009, **113**, 1805–1809.

45. Davies, C. W. The extent of dissociation of salts in water. Part VIII. An equation for the mean ionic activity coefficient of an electrolyte in water, and a revision of the dissociation constants of some sulphates. *J. Chem. Soc.*, 1938, 2093–2098.

46. Sun, M. S., Harriss, D. K. & Magnuson, R. Activity corrections for ionic equilibria in aqueous solutions. *Can. J. Chem.*, 1980, **58**, 1253–1257.

47. Van der Spoel, D. *et al.* GROMACS: Fast, flexible, and free. *J. Comput. Chem.*, 2005, **26**, 1701–1718.

48. Parrinello, M. & Rahman, A. Polymorphic transitions in single crystals: A new molecular dynamics method. *J. Appl. Phys.*, 1981, **52**, 7182–7190.

49. Bussi, G., Donadio, D. & Parrinello, M. Canonical sampling through velocity rescaling. *J. Chem. Phys.*, 2007, **126**, 014101.

50. Darden, T., York, D. & Pedersen, L. Particle mesh Ewald: An Nlog(N) method for Ewald sums in large systems. *J. Chem. Phys.*, 1993, **98**, 10089–10092.

51. Hess, B., Bekker, H., Berendsen, H. J. C. & Fraaije, J. G. E. M. LINCS: A linear constraint solver for molecular simulations. *J. Comput. Chem.*, 1997, **18**, 1463–1472.

52. Miyamoto, S. & Kollman, P. A. SETTLE: an analytical version of the SHAKE and RATTLE algorithm for rigid water models. *J. Comput. Chem.*, 1992, **13**, 952–962.

53. Berendsen, H. J. C., Grigera, J. R. & Straatsma, T. P. The missing term in effective pair potentials. *J. Phys. Chem.*, 1987, **91**, 6269–6271.

54. Joung, I. S. & Cheatham, T. E. Determination of alkali and halide monovalent ion parameters for use in explicitly solvated biomolecular simulations. *J. Phys. Chem. B*, 2008,

112, 9020–9041.

55.   Li, P., Roberts, B. P., Chakravorty, D. K. & Merz, K. M. Rational design of particle mesh ewald compatible lennard-jones parameters for +2 metal cations in explicit solvent. *J.Chem. Theory Comput.*, 2013, **9**, 2733–2748.

56.   Mamatkulov, S., Fyta, M. & Netz, R. R. Force fields for divalent cations based on single-ion and ion-pair properties. *J. Chem. Phys.*, 2013, **138**, 024505.

57.   Callahan, K. M., Casillas-Ituarte, N. N., Roeselová, M., Allen, H. C. & Tobias, D. J. Solvation of magnesium dication: molecular dynamics simulation and vibrational spectroscopic study of magnesium chloride in aqueous solutions. *J. Phys. Chem. A*, 2010, **114**, 5141–5148.

58.   Stote, R. H. & Karplus, M. Zinc binding in proteins and solution: a simple but accurate nonbonded representation. *Proteins*, 1995, **23**, 12–31.

59.   Leontyev, I. V. & Stuchebrukhov, A. A. Electronic continuum model for molecular dynamics simulations. *J. Chem. Phys.*, 2009, **130**, 085102.

60.   Leontyev, I. & Stuchebrukhov, A. Accounting for electronic polarization in non-polarizable force fields. *Phys. Chem. Chem. Phys.*, 2011, **13**, 2613–2626.

61.   Kirby, B. J. & Jungwirth, P. Charge Scaling Manifesto: A Way of Reconciling the Inherently Macroscopic and Microscopic Natures of Molecular Simulations. *J. Phys. Chem. Lett.*, 2019, **10**, 7531–7536.

62.   Kohagen, M., Mason, P. E. & Jungwirth, P. Accounting for Electronic Polarization Effects in Aqueous Sodium Chloride via Molecular Dynamics Aided by Neutron Scattering. *J. Phys. Chem. B*, 2016, **120**, 1454–1460.

63.   Kohagen, M., Mason, P. E. & Jungwirth, P. Accurate description of calcium solvation in concentrated aqueous solutions. *J. Phys. Chem. B*, 2014, **118**, 7902–7909.

64.   Duboué-Dijon, E. Supporting data files for 'Binding of Divalent Cations to Aqueous Acetate: Molecular Simulations Guided by Raman Spectroscopy'. 2020, doi: 10.5281/zenodo.3827165.

65.   Jorgensen, W. L., Buckner, J. K., Boudon, S. & Tirado-Rives, J. Efficient computation of absolute free energies of binding by computer simulations. Application to the methane dimer in water. *J. Chem. Phys.*, 1988, **89**, 3742–3746.

66.   Hermans, J. & Shankar, S. The Free Energy of Xenon Binding to Myoglobin from

Molecular Dynamics Simulation. *Isr. J. Chem.*, 1986, **27**, 225–227.

67. Boresch, S., Tettinger, F., Leitgeb, M. & Karplus, M. Absolute Binding Free Energies: A Quantitative Approach for Their Calculation. *J. Phys. Chem. B*, 2003, **107**, 9535–9551.

68. Roux, B., Nina, M., Pomès, R. & Smith, J. C. Thermodynamic stability of water molecules in the bacteriorhodopsin proton channel: A molecular dynamics free energy perturbation study. *Biophys. J.*, 1996, **71**, 670–681.

69. Bennett, C. H. Efficient estimation of free energy differences from Monte Carlo data. *J. Comput. Phys.*, 1976, **22**, 245–268.

70. de Leeuw, S. W., Perram, J. W. & Smith, E. R. Simulation of Electrostatic Systems in Periodic Boundary Conditions. I. Lattice Sums and Dielectric Constants. *Proc. R. Soc. A Math. Phys. Eng. Sci.*, 1980, **373**, 27–56.

71. Hummer, G., Pratt, L. R. & Angel E. Garcia. On the free energy of ionic hydration. *J. Chem. Phys.*, 1956, **24**, 357–359.

72. Simonson, T. & Roux, B. Concepts and protocols for electrostatic free energies. *Mol. Simul.*, 2016, **42**, 1090–1101.

73. Kumar, M., Simonson, T., Ohanessian, G. & Clavaguéra, C. Structure and thermodynamics of Mg:phosphate interactions in water: A simulation study. *ChemPhysChem*, 2015, **16**, 658–665.

74. Mobley, D. L., Chodera, J. D. & Dill, K. A. On the use of orientational restraints and symmetry corrections in alchemical free energy calculations. *J. Chem. Phys.*, 2006, **125**, 084902.

75. Wang, J., Deng, Y. & Roux, B. Absolute binding free energy calculations using molecular dynamics simulations with restraining potentials. *Biophys. J.*, 2006, **91**, 2798–2814.

76. Vandevondele, J. *et al.* QUICKSTEP: Fast and accurate density functional calculations using a mixed Gaussian and plane waves approach. *Comput. Phys. Comm.*, 2005, **167**, 103–128.

77. Becke, A. D. Density-functional exchange-energy approximation with correct asymptotic behavior. *Phys. Rev. A*, 1988, **38**, 3098–3100.

78. Lee, C., Yang, W. & Parr, R. G. Development of the Colle-Salvetti correlation-energy formula into a functional of the electron density. *Phys. Rev. B*, 1988, **37**, 785–789.

79. Grimme, S., Antony, J., Ehrlich, S. & Krieg, H. A consistent and accurate ab initio

parametrization of density functional dispersion correction (DFT-D) for the 94 elements H-Pu. *J. Chem. Phys.*, 2010, **132**, 154104.

80. Smith, D. G. A., Burns, L. A., Patkowski, K. & Sherrill, C. D. Revised damping parameters for the D3 dispersion correction to density functional theory. *J. Phys. Chem. Lett.*, 2016, **7**, 2197–2203.

81. Becke, A. D. & Johnson, E. R. A density-functional model of the dispersion interaction. *J. Chem. Phys.*, 2005, **123**, 154101.

82. Grimme, S. Semiempirical GGA-type density functional constructed with a long-range dispersion correction. *J. Comput. Chem.*, 2006, **27**, 1787–1799.

83. VandeVondele, J. & Hutter, J. Gaussian basis sets for accurate calculations on molecular systems in gas and condensed phases. *J. Chem. Phys.*, 2007, **127**, 114105.

84. Goedecker, S., Teter, M. & Hutter, J. Separable dual-space Gaussian pseudopotentials. *Phys. Rev. B*, 1996, **54**, 1703–1710.

85. Kumar, S., Rosenberg, J. M., Bouzida, D., Swendsen, R. H. & Kollman, P. A. Multidimensional free-energy calculations using the weighted histogram analysis method. *J. Comput. Chem.*, 1995, **16**, 1339–1350.

86. Grossfield, A. An implementation of WHAM: the weighted histogram analysis method. *Analysis*, 2004, **1**, 1–13.

87. Palivec, V. *et al.* Simulation of Raman and Raman optical activity of saccharides in solution. *PCCP*, 2020, **22**, 1983–1993.

88. Frisch, M. J. *et al.* Gaussian 16 Revision C.01. 2016.

89. Jorgensen, W. L., Chandrasekhar, J., Madura, J. D., Impey, R. W. & Klein, M. L. Comparison of simple potential functions for simulating liquid water. *J. Chem. Phys.*, 1983, **79**, 926.

90. Dapprich, S., Komáromi, I., Byun, K. S., Morokuma, K. & Frisch, M. J. A new ONIOM implementation in Gaussian98. Part I. The calculation of energies, gradients, vibrational frequencies and electric field derivatives. *J. Mol. Struct.*, 1999, **461**–**462**, 1–21.

91. Ruud, K., Helgaker, T. & Bouř, P. Gauge-origin independent density-functional theory calculations of vibrational Raman optical activity. *J. Phys. Chem. A*, 2002, **106**, 7448–7455.

92. Davis, J. G., Zukowski, S. R., Rankin, B. M. & Ben-Amotz, D. Influence of a Neighboring Charged Group on Hydrophobic Hydration Shell Structure. *J. Phys. Chem. B*, 2015, **119**,

9417–9422.

93.   Quilès, F., Burneau, A. & Gross, N. Vibrational spectroscopic study of the complexation of mercury(II) by substituted acetates in aqueous solutions. *Appl. Spectrosc.*, 1999, **53**, 1061–1070.

94.   Uejio, J. S. *et al.* Characterization of selective binding of alkali cations with carboxylate by X-ray absorption spectroscopy of liquid microjets. *Proc. Natl. Acad. Sci.*, 2008, **105**, 6809–6812.

95.   Atkinson, G., Emara, M. M. & Fernández-Prini, R. Ultrasonic absorption in aqueous solutions of calcium acetate and other bivalent metal acetates. *J. Phys. Chem.*, 1974, **78**, 1913–1917.

96.   Duboué-Dijon, E. *et al.* Binding of divalent cations to insulin: capillary electrophoresis and molecular simulations. *J. Phys. Chem. B*, 2018, **122**, 5640–5648.

97.   Ponder, J. W. *et al.* Current status of the AMOEBA polarizable force field. *J. Phys. Chem. B*, 2010, **114**, 2549–2564.

98.   Villa, F., Mackerell, A. D., Roux, B. & Simonson, T. Classical Drude Polarizable Force Field Model for Methyl Phosphate and Its Interactions with Mg2+. *J. Phys. Chem. A*, 2018, **122**, 6147–6155.

99.   Lemkul, J. A., Huang, J., Roux, B. & Mackerell, A. D. An Empirical Polarizable Force Field Based on the Classical Drude Oscillator Model: Development History and Recent Applications. *Chem. Rev.*, 2016, **116**, 4983–5013.

100.   Simonson, T. & Satpati, P. Simulating GTP:Mg and GDP:Mg with a simple force field: A structural and thermodynamic analysis. *J. Comput. Chem.*, 2013, **34**, 836–846.

101.   Kann, Z. R. & Skinner, J. L. A scaled-ionic-charge simulation model that reproduces enhanced and suppressed water diffusion in aqueous salt solutions. *J. Chem. Phys.*, 2014, **141**, 104507.

102.   Zeron, I. M., Abascal, J. L. F. & Vega, C. A force field of Li , Na , K , Mg , Ca , in aqueous solution based on the TIP4P / 2005 water model and scaled charges for the ions in aqueous solution based on the TIP4P / 2005 water model and scaled charges for the ions. *J. Chem. Phys.*, 2019, **151**, 134504.

103.   Caminiti, R., Licheri, G., Piccaluga, G. & Pinna, G. X-ray diffraction study of MgCl2 aqueous solutions. *J. Appl. Cryst.*, 1979, **12**, 34–38.

104. Katz, A. K., Glusker, J. P., Beebe, S. A. & Bock, C. W. Calcium ion coordination: A comparison with that of beryllium, magnesium, and zinc. *J. Am. Chem. Soc.*, 1996, **118**, 5752–5763.

105. Daily, M. D., Baer, M. D. & Mundy, C. J. Divalent Ion Parameterization Strongly Affects Conformation and Interactions of an Anionic Biomimetic Polymer. *J. Phys. Chem. B*, 2016, **120**, 2198–2208.

106. Shannon, R. D. Revised Effective Ionic Radii and Systematic Studies of Interatomie Distances in Halides and Chaleogenides. *Acta Cryst. A*, 1976, **32**, 751–767.

107. Shannon, R. D. & Fischer, R. X. Empirical electronic polarizabilities of ions for the prediction and interpretation of refractive indices: Oxides and oxysalts. *Am. Mineral.*, 2016, **101**, 2288–2300.

108. Linstrom, P. J. & Mallard, W. G. *NIST Chemistry WebBook, NIST Standard Reference Database Number 69*. National Institute of Standards and Technology, Gaithersburg MD, 20899.